Journal of Solid State Chemistry 183 (2010) 727–735

Contents lists available at ScienceDirect

Journal of Solid State Chemistry

journal homepage: www.elsevier.com/locate/jssc

Synthesis, structures, and phase transitions of barium bismuth iridium oxide perovskites Ba_2BiIrO_6 and $Ba_3BiIr_2O_9$

Chris D. Ling [a,b,*], Brendan J. Kennedy [a], Qingdi Zhou [a], Jarrah R. Spencer [c], Maxim Avdeev [b]

[a] School of Chemistry, The University of Sydney, Sydney 2006, Australia
[b] Bragg Institute, ANSTO, PMB 1, Menai 2234, Australia
[c] Department of Pharmacology, The University of Sydney, Sydney 2006, Australia

ARTICLE INFO

Article history:
Received 18 December 2009
Received in revised form
14 January 2010
Accepted 18 January 2010
Available online 25 January 2010

Keywords:
Double perovskite
Hexagonal perovskite
Synchrotron XRD
Neutron powder diffraction
Rietveld-refinement
Iridium oxides
Phase transitions

ABSTRACT

The Ba–Bi–Ir–O system is found to contain two distinct perovskite-type phases: a rock-salt ordered double perovskite Ba_2BiIrO_6; and a 6H-type hexagonal perovskite $Ba_3BiIr_2O_9$. Ba_2BiIrO_6 undergoes a series of symmetry-lowering phase transitions on cooling $Fm\bar{3}m \rightarrow R\bar{3}c \rightarrow 12/m(C2/m) \rightarrow I\bar{1}(P\bar{1})$, all of which are second order except the rhombohedral → monoclinic one, which is first order. The monoclinic phase is only observed in a 2-phase rhombohedral+monoclinic regime. The transition and 2-phase region lie very close to 300 K, making the room-temperature X-ray diffraction patterns extremely complex and potentially explaining why Ba_2BiIrO_6 had not previously been identified and reported. A solid solution $Ba_2Bi_{1+x}Ir_{1-x}O_6$, analogous to $Ba_2Bi_{1+x}Ru_{1-x}O_6$, $0 \le x \le 2/3$, was not observed. The 6H-type phase $Ba_3BiIr_2O_9$ undergoes a clean second-order phase transition $P6_3/mmc \rightarrow C2/c$ at 750 K, unlike 6H-type $Ba_3LaIr_2O_9$, the $P6_3/mmc$ structure of which is highly strained below ~750 K but fails to distort coherently to the monoclinic phase.

1. Introduction

To the best of our knowledge, there are no direct reports in the literature of any phases in the Ba–Bi–Ir–O system. This is rather surprising, given the large number of well-characterized phases in chemically very similar systems. Double perovskites Ba_2MIrO_6 are known for 3+valent cations M=In, Sc, Y, La, and many of the rare earths [1–4], but not M=Bi. 6H-type perovskites $Ba_3MIr_2O_9$ are known for essentially the same range of M [1,5–7], again with the exception of M=Bi. The omission is particularly striking in the case of the 6H perovskites, given that $Ba_3BiRu_2O_9$ [8] and $Ba_3BiRuIrO_9$ [9] have been reported. Lufaso et al. [9] use $Ba_3BiIr_2O_9$ as an example of a 6H-type perovskite with $C2/c$ space group symmetry, but the cited reference [6] does not actually mention this phase. Thus, while it seems highly likely that Ba–Bi–Ir–O perovskites have been encountered and at least partially characterized at some time by the authors cited above and/or others, those phases have never been formally described.

The most likely explanation for the absence of Ba–Bi–Ir–O perovskites from the literature is that they are difficult or impossible to synthesize as pure compounds. This would greatly complicate the structural and magnetic property characterization normally required for publication. A hint of the potential difficulties is given by the ruthenium analogs, notably the report by Darriet et al. [8] that the double perovskite $Ba_2Bi_{2-x}Ru_xO_6$ only exists for $x \le 0.67$; attempts to synthesize Ba_2BiRuO_6 lead instead to a mixture consisting mostly of $Ba_2Bi_{1.33}Ru_{0.67}O_6$ and $Ba_3BiRu_2O_9$.

The Ba_2MIrO_6 and $Ba_3MIr_2O_9$ phases described in the articles cited above exhibit quite interesting magnetic and electronic behavior, especially the 6H-type phases, which show magnetic ordering of the spins (S=1/2) on $Ir^{4.5+}$ within face-sharing octahedral dimers Ir_2O_9. Moreover, the stereochemically active $6s^2$ electron lone pair on Bi^{3+} often results in different structural distortions and therefore different magnetic properties compared to other M^{3+} cations. This motivated the study described in this article: a careful investigation of the Ba–Bi–Ir–O system in order to identify, purify, and characterize the structures of any previously unreported perovskite-type phases.

2. Experimental

Reaction progress was followed by conventional (Cu$K\alpha$) X-ray diffraction (XRD) on a Panalytical X'Pert Pro diffractometer equipped with a PIXcel detector. All syntheses were conventional solid-state reactions using reagents ($BaCO_3$, Bi_2O_3, and Ir metal)

* Corresponding author at: School of Chemistry, The University of Sydney, Sydney 2006, Australia.
E-mail address: c.ling@chem.usyd.edu.au (C.D. Ling).

0022-4596/$ - see front matter © 2010 Elsevier Inc. All rights reserved.
doi:10.1016/j.jssc.2010.01.017

purchased from commercial suppliers of 99.98 % or greater purity. $BaCO_3$ was dried at 1000 K overnight before use.

Initial attempts to synthesize Ba_2BiIrO_6 from a stoichiometric (in terms of metal atom ratios) mixture of reagents led to the results expected, based on the reports of the ruthenium analog [8]. A mixture of phases was observed in the XRD patterns, which could be mostly indexed to a double-perovskite phase (presumably $Ba_2Bi_{2-x}Ir_xO_6$) and a 6H-type phase (presumably $Ba_3BiIr_2O_9$), as well as a few very weak peaks that were difficult to assign. The synthesis was therefore repeated with the stoichiometry adjusted to $Ba_2Bi_{2-x}Ir_xO_6$, x=0.67. However, rather than eliminating the 6H-type phase as expected, XRD patterns showed that this led to essentially the same ratio of phases in the product. We then repeated our attempt to synthesize Ba_2BiIrO_6 with a 10% excess of Bi_2O_3 added to compensate for the possible evaporation of Bi_2O_3 above its melting point of 1090 K (a commonly observed phenomenon). XRD showed that this approach produced a pure double-perovskite phase after annealing at 873 K/16 h, 1273 K/16 h, 1423 K/20 h, and 1073 K/15 days with intermediate regrinding and pelletization.

The same procedure was successfully adapted to synthesize a pure sample at the stoichiometry of the presumed 6H-type phase $Ba_3BiIr_2O_9$; however, it was found that an excess of Bi_2O_3 was not required in this case. Stoichiometric (in terms of metal atoms) mixtures of reagents were ground together in an agate mortar and heated to 1073 K for 12 h in an alumina crucible as a first step to remove CO_2. Samples were then reground, pelletized and gradually heated from 750 to 800 K over 5 days, then reground and pelletized again and annealed at 1400 K for 7 days (covered) with several intermediate regrindings. All heating procedures were carried out under air. Finally, as a reference for the 6H-type structure, we also synthesized a sample of $Ba_3LaIr_2O_9$ using the equivalent method.

Variable temperature synchrotron XRD (S-XRD) data were collected at the Powder Diffraction Beamline of the Australian Synchrotron at a wavelength of λ=0.689079 Å (calibrated against a LaB_6 standard). Samples were placed in unsealed 0.3 mm diameter quartz capillaries, which were heated with a hot air blower and/or cooled with a liquid nitrogen cryostream.

Neutron powder diffraction (NPD) data were collected on the instrument Echidna at the OPAL research reactor, Lucas Heights, Australia at 1.6215 and 2.4395 Å. Samples were placed in 9 mm diameter vanadium cans. Low temperature data were collected in a standard "Orange" helium cryostat.

Rietveld-refinements against S-XRD and NPD data were carried out using the Rietica program [10] and the GSAS program [11] with the EXPGUI front-end [12]. Scale factors, zero-shifts, background functions, and pseudo-Voigt peak shape parameters were

Table 1
Final structural parameters and empirical bond valence sums (BVS) [17] for Ba_2BiIrO_6 at representative temperatures within each phase regime, obtained by Rietveld-refinement against S-XRD data. All site occupancies are 100%.

	$x(a)$	$y(b)$	$z(c)$	Site	$100U_{eq}$	BVS
T=500 K: space group $Fm\bar{3}m$ (#225), Z=4, a=8.51779(2) Å, V=617.989(4) Å^3						
Ba1	1/4	1/4	1/4	8*c*	1.00(2)	1.65
Bi1	0	0	0	4*a*	0.78(3)	3.06
Ir1	1/2	1/2	1/2	4*b*	0.33(5)	5.64
O1	0.2751(7)	0	0	24*e*	1.0(3)	2.00
T=300 K: space group $R\bar{3}c$ (#167), Z=3, a=6.00460(3), c=14.7497(7) Å, V=460.531(6) Å^3						
Ba1	0	0	0.2562(5)	12*c*	0.59(4)	1.73
Bi1	0	0	0	6*b*	0.56(7)	3.53
Ir1	0	0	1/2	6*b*	0.59(5)	4.82
O1	0.5160(7)	0.9871(10)	0.2378(3)	36*f*	0.9(2)	1.97
T=80 K: space group $I\bar{1}$ (#2), Z=2, a=5.99322(8), b=5.99181(9), c=8.49376(14) Å, α=90.1435(12), β=90.4939(10)°, γ=89.8091(12)°, V=304.901(8) Å^3						
Ba1	0.5002(15)	0.4994(15)	0.2493(8)	2*i*	0.55(10)	1.95
Bi1	0	1/2	0	1*c*	0.91(6)	2.93
Ir1	1/2	0	0	1*d*	0.74(6)	5.74
O1	0.264(2)	0.218(2)	1.0377(17)	2*i*	−1.13(11)[a]	2.05
O2	0.291(3)	0.786(3)	0.0223(19)	2*i*	−0.76(15)[a]	2.23
O3	0.544(3)	0.037(3)	0.2319(15)	2*i*	−1.00(11)[a]	2.01

[a] The negative ADPs on oxygen atoms at 80 K are an artifact due to absorption and the poor relative sensitivity of X-rays to oxygen atoms in the presence of very heavy metal cations.

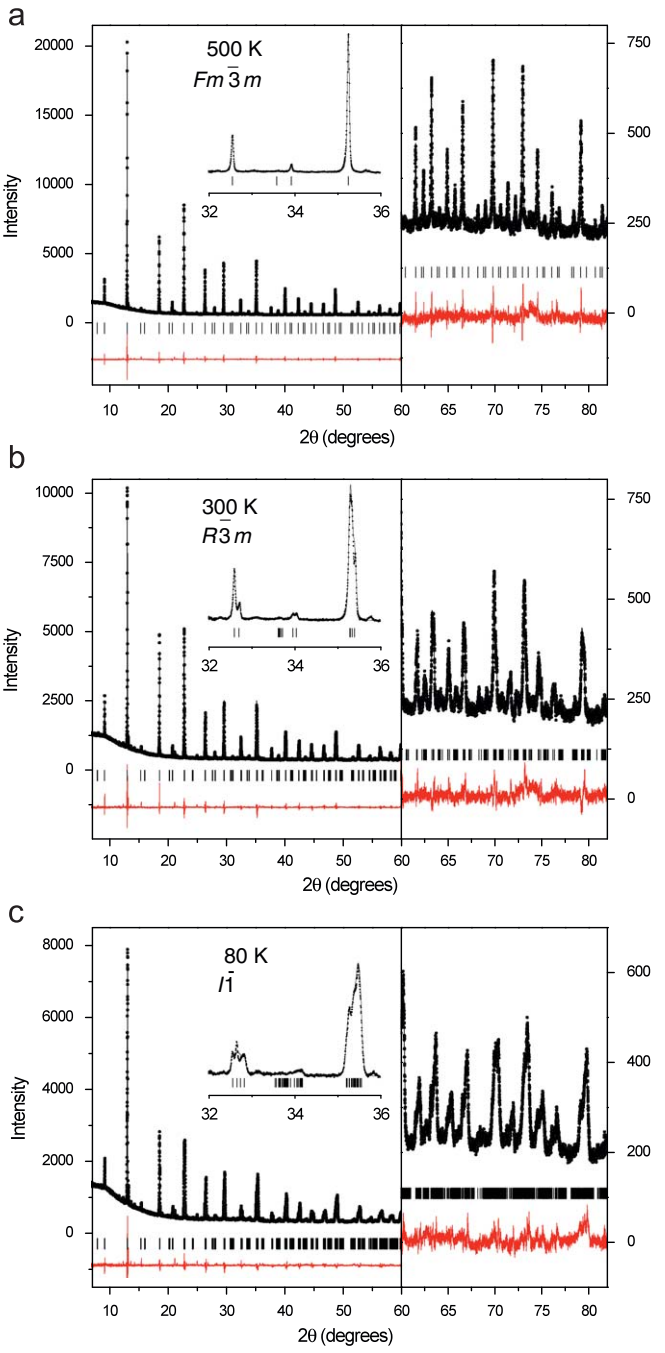

Fig. 1. Observed (crosses), calculated (upper line) and difference (lower line) profiles for the final Rietveld-refinements against S-XRD data (l=0.6891 Å) of Ba_2BiIrO_6 at (a) 500 K, (b) 300 K, and (c) 80 K. Note the changes in scale at 2θ=60°. The insets show the splitting of the Bragg reflections consistent with cubic symmetry at 500 K, rhombohedral symmetry at 300 K, and monoclinic symmetry at 80 K.

Table 2
Final structural parameters and BVS for $Ba_3BiIr_2O_9$ at room temperature, obtained by Rietveld-refinement simultaneously against NPD and S-XRD data. All site occupancies are 100%.

	$x(a)$	$y(b)$	$z(c)$	Site	$100U_{eq}$	BVS
Space group $C2/c$ (#15), $Z=4$, $a=5.953094(15)$, $b=10.27922(2)$, $c=14.88920(4)$ Å, $\beta=91.9337(2)^\circ$, $V=910.598(4)$ Å^3						
Ba1	0	0.9950(2)	0.25	4*e*	1.41	1.94
Ba2	0.00954(19)	0.3329(2)	0.09556(8)	8*f*	1.58	1.81
Bi1	0	0	0	4*a*	1.11	3.68
Ir1	0.98389(11)	0.33473(11)	0.83723(5)	8*f*	0.95	4.52
O1	0	0.5109(5)	0.25	4*e*	2.88	1.94
O2	0.5347(7)	0.3255(4)	0.0917(2)	8*f*	2.13	2.05
O3	0.2696(5)	0.2400(3)	0.2391(2)	8*f*	1.45	2.00
O4	0.7725(6)	0.0891(4)	0.1007(3)	8*f*	2.23	2.12
O5	0.6898(6)	0.0912(4)	0.4256(2)	8*f*	2.40	2.00
	U_{11}	U_{12}	U_{13}	U_{22}	U_{23}	U_{33}
Ba1	0.0213(9)	0.0	−0.0022(6)	0.0119(9)	0.0	0.0088(8)
Ba2	0.0140(6)	−0.0008(5)	−0.0019(5)	0.0163(6)	0.0002(5)	0.0168(6)
Bi1	0.0131(5)	0.0000(4)	−0.0008(4)	0.0155(6)	0.0004(4)	0.0046(4)
Ir1	0.0102(3)	−0.0001(3)	−0.0003(2)	0.0109(3)	0.0005(3)	0.0073(3)
O1	0.028(3)	0.0	0.024(2)	0.022(3)	0.0	0.037(3)
O2	0.025(2)	0.0053(15)	0.0012(13)	0.0099(17)	0.0107(14)	0.0288(19)
O3	0.0026(14)	0.0015(12)	0.0063(13)	0.0062(14)	0.0011(14)	0.035(2)
O4	0.015(2)	0.0087(16)	0.0058(14)	0.029(2)	0.0038(16)	0.0224(19)
O5	0.0179(17)	0.0011(16)	−0.0026(15)	0.025(2)	0.0107(15)	0.0283(19)

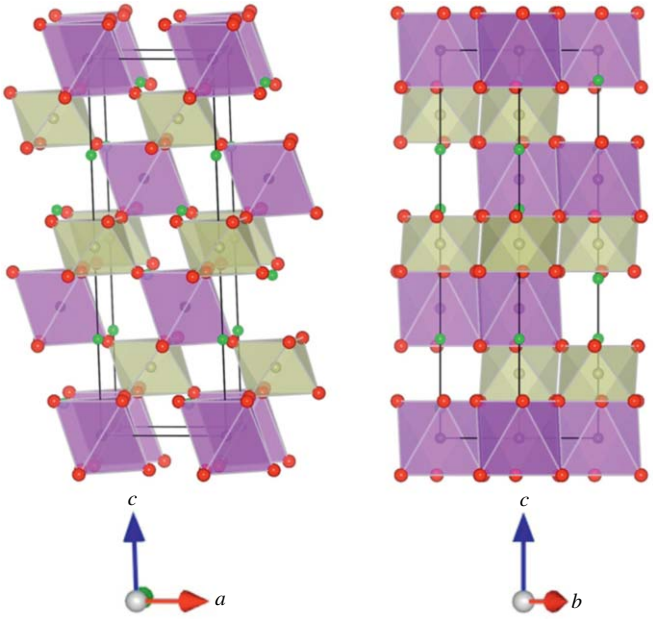

Fig. 2. Structure of Ba_2BiIrO_6 as Rietveld-refined against NPD data in $R\bar{3}c$ at 300 K. BiO_6 octahedra are blue, IrO_6 octahedra are gold, and Ba atoms are green. Anisotropic ADPs are shown as thermal ellipsoids at 90% probability. (For interpretation of the references to color in this figure legend, the reader is referred to the web version of this article.)

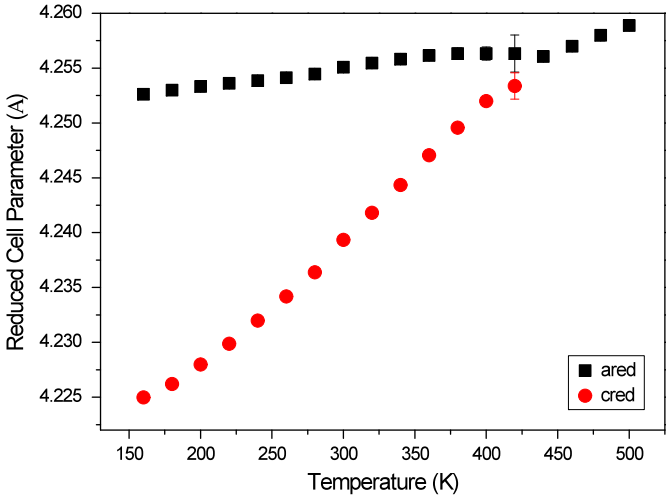

Fig. 3. Temperature dependence of the appropriately scaled lattice parameters in Ba_2BiIrO_6 between 180 and 500 K obtained by Rietveld analysis of S-XRD data. The transition to cubic is evident near 450 K. The fits to the profiles at 140 and 160 K revealed the co-existence of a monoclinic phase.

refined in addition to the structural parameters described in Section 3 below.

3. Results

3.1. Ba_2BiIrO_6

The synchrotron powder diffraction pattern of Ba_2BiIrO_6 recorded at 500 K was indexed to a F-centered cubic cell with $a=8.51779(2)$ Å, as expected for a rock-salt ordered double perovskite. The structure was Rietveld-refined against S-XRD data using the Rietica program in space group $Fm\bar{3}m$, using $Ba_2Bi^{3+}Bi^{5+}O_6$ [13] as a starting model. The results are summarized in Table 1 and the final fit illustrated in Fig. 1(a). Final refinement statistics: $R_p=0.0450$, $WR_p=0.0644$, $R(F^2)=0.0134$ for 152 observations, $\chi^2=7.10$ for 13 variables. The refined Bi–O distance of 2.343(6) Å and Ir–O distance of 1.915(6) Å are typical for Ir^{5+} and Bi^{3+} in perovskites (e.g. $Ba_2Bi^{3+}Bi^{5+}O_6$ [13], Ba_2LaIrO_6 [14]).

Cooling the sample below 450 K resulted in the broadening, and then splitting, of selected reflections indicative of a structural phase transition. Based on the observed splitting the appropriate space group was identified as $R\bar{3}c$, as for Ba_2LaIrO_6 [14]. The room-temperature structure of Ba_2BiIrO_6 was Rietveld-refined against S-XRD data using the Rietica program, with the results summarized in Table 2 and the final fit illustrated in

Fig. 1(b). The structure is shown in Fig. 2. Final refinement statistics: R_p=0.0520, WR_p=0.0700, $R(F^2)$=0.1465 for 793 observations, χ^2=1.57 for 24 variables.

The refined Bi–O distance of 2.290(6) Å and Ir–O distance of 1.974(6) Å are unexceptional, the small increase in the Ir–O distance compared to the 500 K value simply reflecting the difficulties associated with refining accurate atomic coordinates for light elements such as oxygen in the presence of very heavy metal cations using XRD data.

The temperature dependence of the lattice parameters between 160 and 500 K is shown in Fig. 3. It is apparent that the $R\bar{3}c \rightarrow Fm\bar{3}m$ transition is continuous as allowed by group theory [15]. The temperature dependence of the structure below 160 K is more complex. In Fig. 4, a slight shoulder is apparent on the low-angle side of the (404) reflection. There is also an increase in intensity between the (404) and (0,0,12) reflections, and a change in the relative intensities of the multiplet derived from the $(400)_p$ (where the subscript "p" denotes the primitive cubic perovskite cell) reflection near 2θ=35.5°. We believe that these changes reflect the co-existence of a second phase (monoclinic $I2/m$) with the rhombohedral phase. These two phases appear to co-exist over a narrow temperature range (140–160 K). Given the complexity of this two-phase mixture, a full Rietveld-refinement of the monoclinic phase was not attempted.

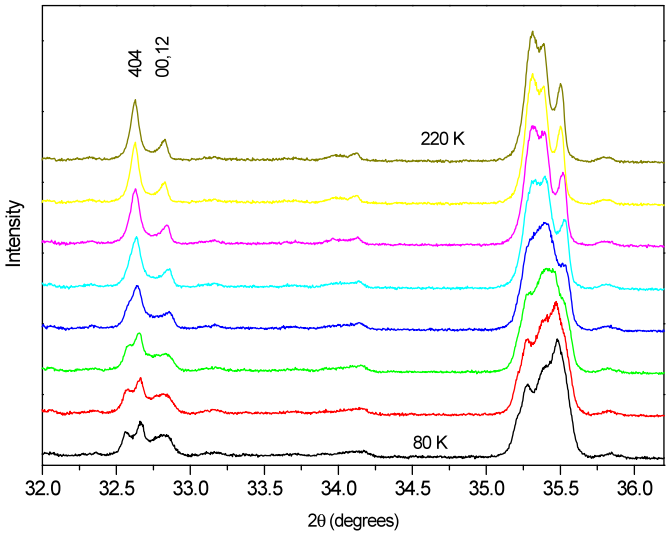

Fig. 4. Portions of the observed S-XRD patterns (λ=0.6891 Å) of Ba_2BiIrO_6 obtained at 20 K intervals from 80 K (bottom trace) to 220 K (upper trace).

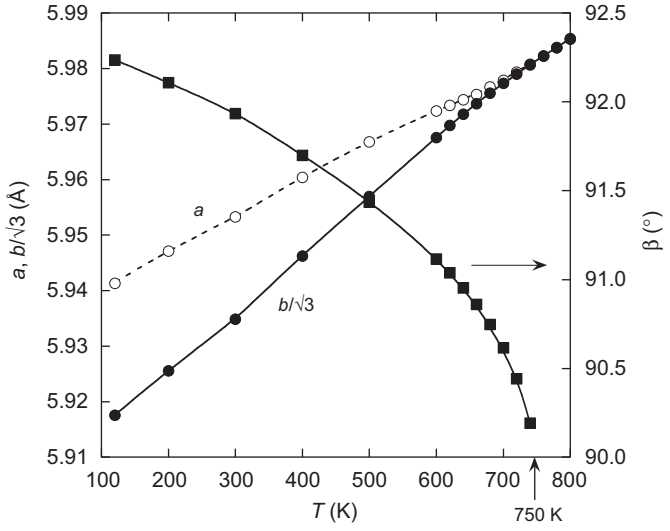

Fig. 5. Unit cell parameters *vs.* temperature for $Ba_3BiIr_2O_9$ in terms of the low-temperature $C2/c$ room-temperature cell, as determined by Rietveld-refinement of S-XRD data.

At 100 K the appearance of the pattern changes again: the rhombohedral (0,0,12) reflection is noticeably broader than the pair of peaks derived from the (404) reflection, suggesting this may also be a doublet. This is inconsistent with a monoclinic model and suggests a further lowering of symmetry. Given that no M or X-point reflections are observed in the diffraction pattern, it seems likely that the low temperature structure is triclinic $I\bar{1}$. The triclinic structure was Rietveld-refined against S-XRD data using the Rietica program in space group $Fm\bar{3}m$, with the results summarized in Table 1 and the final fit illustrated in Fig. 1(c). Final refinement statistics: R_p=0.0421, WR_p=0.0592, $R(F^2)$=0.0120 for 2288 observations, χ^2=9.90 for 32 variables.

3.2. $Ba_3BiIr_2O_9$

Variable temperature S-XRD data showed a clear phase transition at 750 K. Above this temperature, $Ba_3BiIr_2O_9$ has the ideal 6H-type space group symmetry $P6_3/mmc$. Below, peak splitting and systematic absences indicate the monoclinic space group $C2/c$, which is reported at room temperature for a number of 6H-type compounds with Ba in the A-site, notably the highly analogous $Ba_3BiRu_2O_9$ [8], $Ba_3LaIr_2O_9$ and $Ba_3NdIr_2O_9$ [6]. Fig. 5 shows unit cell parameters *vs.* temperature for $Ba_3BiIr_2O_9$ in terms of the low-temperature $C2/c$ cell, as determined by Rietveld-refinement of S-XRD data.

A full Rietveld-refinement, including anisotropic ADPs, was carried out in $C2/c$ at room temperature simultaneously against NPD and S-XRD data using GSAS, using $Ba_3SrSb_2O_9$ [16] as a starting model. The results are summarized in Table 2, with full details available in the deposited CIF file associated with this article. Fig. 6 shows the final Rietveld fits, and Fig. 7 shows the refined structure. Final refinement statistics: R_p=0.0314, WR_p=0.0465, $R(F^2)$=0.1006 for 3371 observations for S-XRD data; R_p=0.0369, WR_p=0.0468, $R(F^2)$=0.0365 for 899 observations for NPD data; χ^2=0.7032 for 135 variables.[1]

3.3. $Ba_3LaIr_2O_9$

S-XRD data for $Ba_3LaIr_2O_9$ could be indexed in $P6_3/mmc$ at room temperature, but with very significant strain-broadening of certain peaks. Fig. 8 shows part of the variable temperature S-XRD patterns; note the broadening of the (217)/(1,0,10) reflections on heating, in contrast to the lack of broadening of the (220) reflection. This indicates significant strain along the z direction, which could be explained by a locally disordered version of the distortions to $C2/c$ seen in $Ba_3BiIr_2O_9$ (Fig. 7), but not by the commonly observed alternative distortion pathway to $P6_3/m$ (rotations around z) [26]. The (217)/(1,0,10) reflections should split on cooling through a second-order transition to monoclinic $C2/c$, but in this case no clean transition is observed. Above ~700 K the width of all reflections become comparable, and the structure can be considered to be well ordered in $P6_3/mmc$.

A full Rietveld-refinement, including anisotropic ADPs, was carried out in $P6_3/mmc$ at 700 K against S-XRD data using GSAS.

[1] Note that the value of $\chi^2 < 1$ arises because, due to technical difficulties, it was not possible to subtract an experimental background from the S-XRD data. This led to the overestimation of $\sigma(I)=I^{1/2}$ for each data point and hence an overestimation of R_{exp}, and ultimately to $\chi^2=[WR_p/R_{exp}]^2 < 1$.

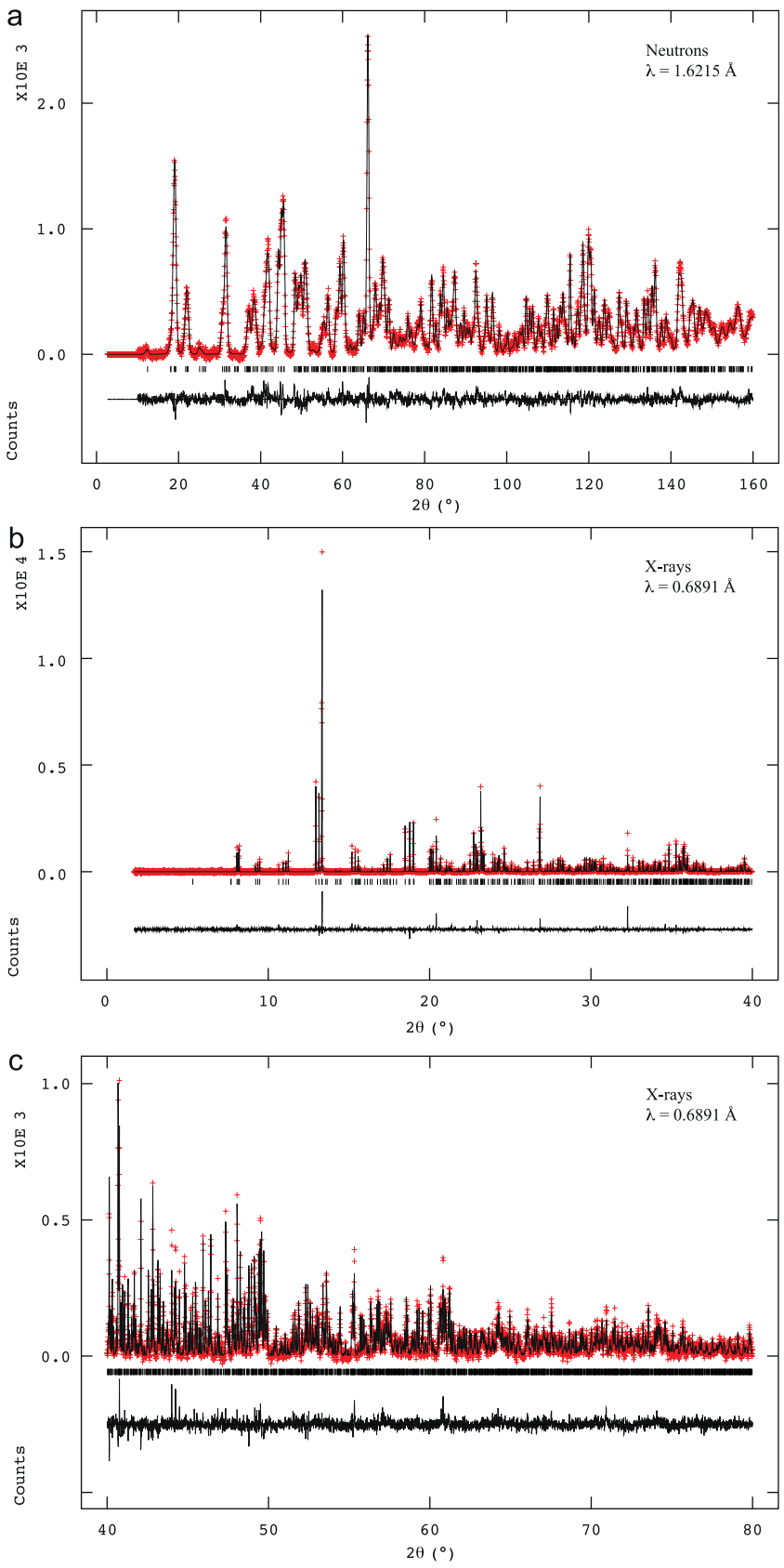

Fig. 6. Observed (crosses), calculated (upper line) and difference (lower line) profiles for the final Rietveld-refinement of $Ba_3BiIr_2O_9$ in *C*2/*c* at 300 K against (a) NPD, and (b,c) S-XRD data.

The results are summarized in Table 3, with full details available in the deposited CIF file associated with this article. Fig. 9 shows the final Rietveld fits, and Fig. 10 shows the refined structure. Final refinement statistics: R_p=0.0434, WR_p=0.0680, $R(F^2)$=0.1305 for 748 observations, χ^2=1.311 for 46 variables.

4. Discussion

The absence of any previous reports in the literature on Ba_2BiIrO_6, despite the high likelihood of it having been previously synthesized, is probably due to the difficulties involved in its synthesis as a pure compound and its structural characterization at room temperature. Even with a pure sample, room temperature XRD data are broadened relative to ideal cubic form, but not sufficiently that the symmetry can be unambiguously determined. In this study, temperature-dependent S-XRD data were required to unambiguously show that on cooling, Ba_2BiIrO_6 undergoes a sequence of phase transitions $Fm\bar{3}m \rightarrow R\bar{3}c \rightarrow I2/m(C2/m) \rightarrow I\bar{1}(P\bar{1})$. This is consistent with the group–subgroup relations for double perovskites determined by Howard et al. [15] and outlined in Fig. 1 of that work, according to which all these transitions can be continuous except for the rhombohedral→monoclinic one, which must be first order. Indeed, the discontinuous nature of that transition is clearly shown by the presence of a distinct 2-phase rhombohedral+monoclinic temperature regime which cedes directly to the pure triclinic phase. The symmetry lowering sequence is very similar to that observed in $Ba_2Bi^{3+}Bi^{5+}O_6$ [13], the only difference being the lowest temperature phase which is $P2_1/n$ instead of $I\bar{1}$.

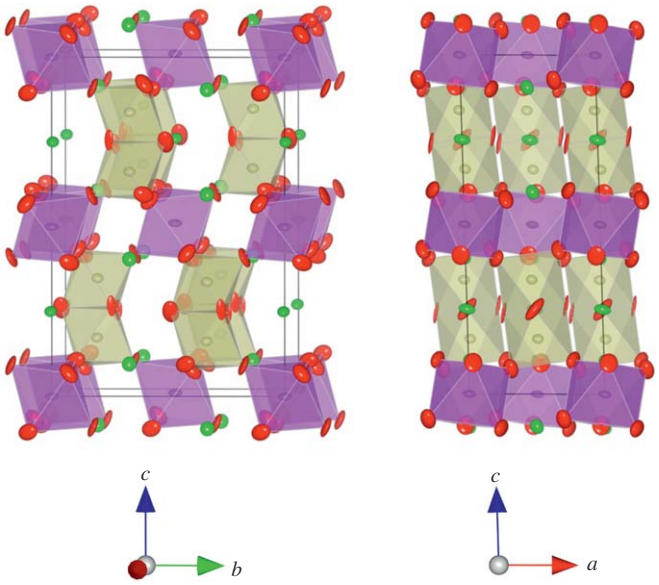

Fig. 7. Structure of $Ba_3BiIr_2O_9$ as Rietveld-refined against S-XRD and NPD data in $C2/c$ at 300 K. BiO_6 octahedra are purple, IrO_6 octahedra are gold, and Ba atoms are green. Anisotropic ADPs are shown as thermal ellipsoids at 90% probability. (For interpretation of the references to color in this figure legend, the reader is referred to the web version of this article.)

Empirical bond valence sums (BVS) [17] were calculated and included in Table 2, using r_0=1.893 for $Ir^{4.5+}$ (taken as the mean of those tabulated for Ir^{5+} and Ir^{4+}). BVS values for Bi^{3+} and O^{2-} ions are reasonable for all three refined phases. However, the BVS value for Ba^{2+} improves with successive symmetry lowering from cubic (1.65) to rhombohedral (1.73) to triclinic (1.95). This drop is much greater than could be explained by thermal expansion (noting that the r_0 values used were compiled from room temperature structures), and suggests that underbonding of the perovskite A-site is the driving force behind these distortions. Note that it is not appropriate to make strong inferences based on the BVS values for $Ir^{4.5+}$, as the value used for r_0=1.893 was taken from the mean of those tabulated for Ir^{5+} and Ir^{4+}, which are themselves poorly defined and largely untested.

Some comment must be made on the lack of evidence for a solid solution $Ba_2Bi_{1+x}Ir_{1-x}O_6$, such as would be expected by analogy with $Ba_2Bi_{1+x}Ru_{1-x}O_6$, $0 \le x \le 2/3$ [8]. We could only successfully synthesize the x=0 phase, which was unexpected given that the x=0 phase in the Ru^{5+} system is reported to prefer

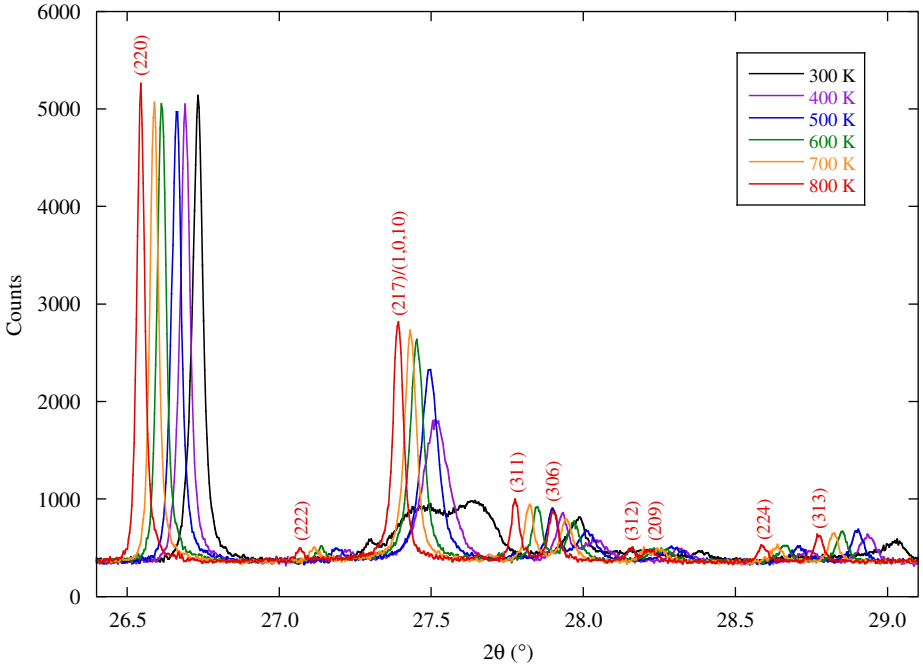

Fig. 8. Part of the S-XRD patterns (λ=0.6891 Å) for $Ba_3LaIr_2O_9$, showing the increase in crystallinity on heating. Indexing corresponds to the $P6_3/mmc$ cell at 800 K.

Table 3
Final structural parameters and BVS for $Ba_3LaIr_2O_9$ at 700 K, obtained by Rietveld-refinement against S-XRD data. All site occupancies are 100%.

	$x(a)$	$y(b)$	$z(c)$	Site	$100U_{eq}$	BVS
Space group $P6_3/mmc$ (#194), Z=2, a=5.99737(3), c=15.14949(9) Å, V=471.900(4) Å^3						
Ba1	0	0	3/4	2*b*	4.11	1.65
Ba2	2/3	1/3	0.89698(11)	4*f*	5.27	1.52
La1	0	0	0	2*a*	2.97	3.23
Ir1	2/3	1/3	0.16443(5)	4*f*	2.58	5.41
O1	0.0373(17)	0.5186(9)	3/4	12*j*	4.23	2.08
O2	0.1849(10)	0.8151(10)	0.9049(6)	12*k*	6.87	2.07
	U_{11}	U_{12}	U_{13}	U_{22}	U_{23}	U_{33}
Ba1	0.0403(8)	0.0202(4)	0	0.0403(8)	0	0.0417(16)
Ba2	0.0378(5)	0.0189(2)	0	0.0378(5)	0	0.0817(14)
La1	0.0294(6)	0.0147(3)	0	0.0294(6)	0	0.0297(13)
Ir1	0.0237(2)	0.01185(11)	0	0.0237(2)	0	0.0296(4)
O1	0.022(6)	0.011(3)	0	0.027(5)	0	0.074(11)
O2	0.050(4)	−0.002(5)	−0.006(3)	0.050(4)	0.006(3)	0.072(9)

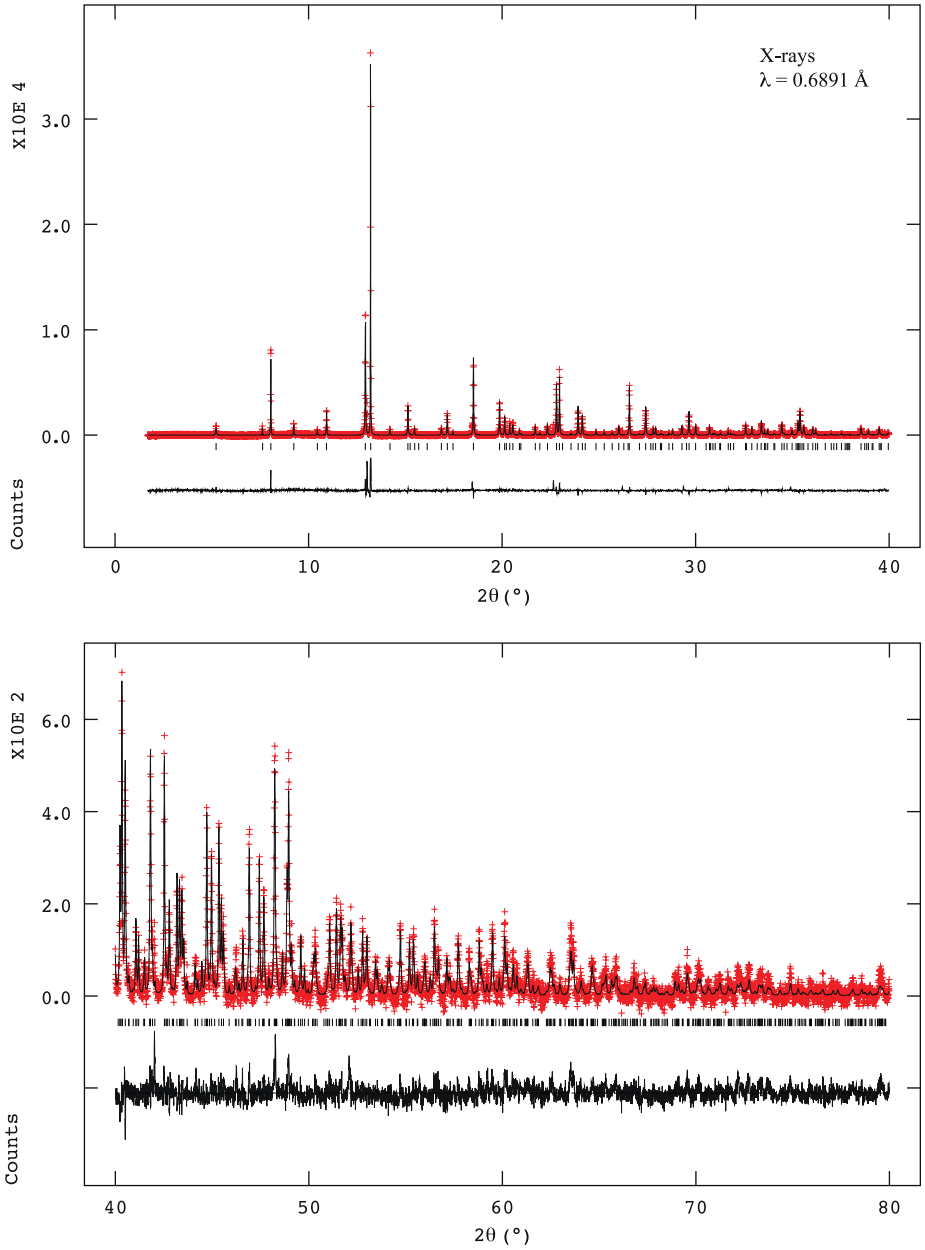

Fig. 9. Observed (crosses), calculated (upper line) and difference (lower line) profiles for the final Rietveld-refinement against S-XRD data of $Ba_3LaIr_2O_9$ in $P6_3/mmc$ at 700 K.

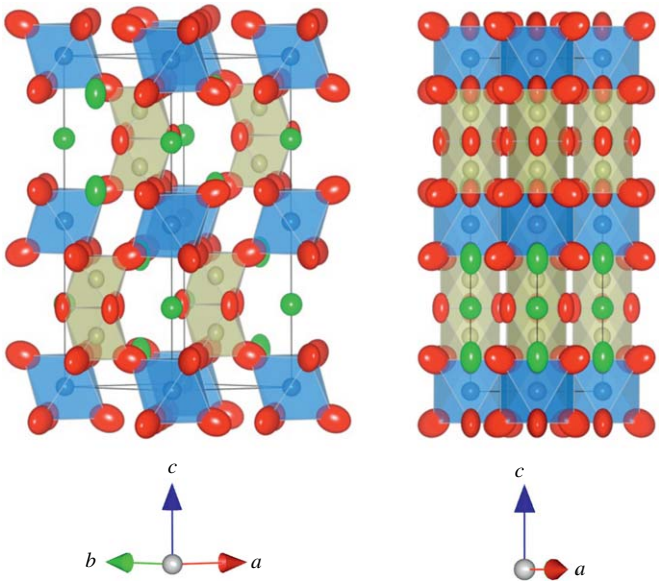

Fig. 10. Structure of $Ba_3LaIr_2O_9$ as Rietveld-refined against S-XRD data in $P6_3/mmc$ at 700 K. LaO_6 octahedra are blue, IrO_6 octahedra are gold, and Ba atoms are green. Anisotropic ADPs are shown as thermal ellipsoids at 90% probability. (For interpretation of the references to color in this figure legend, the reader is referred to the web version of this article.)

an 8H-type hexagonal perovskite structure over the 2C-type double-perovskite structure found in the solid-solution regime [18]. Based on simple ionic size and charge considerations, it is not clear why the Ru^{5+} and Ir^{5+} systems behave so differently; or, indeed, why the chemically closely related phases $Ba_3BiRu_2O_9$ [8] and $Ba_3BiIrRuO_9$ [19] adopt the 6H-type structure. A more detailed investigation of the pseudo-ternary $BaBiO_3$–$BaIrO_3$–$BaRuO_3$ phase diagram would be required to shed light on these differences.

Concerning the structural results presented above for $Ba_3BiIr_2O_9$, group-theoretical analysis using the program *AMPLIMODES* [20] confirmed the plausibility of a direct second-order phase transition from $P6_3/mmc$ to $C2/c$, *via* a Γ^{-6+} soft mode. Two possible intermediate phases exist between $P6_3/mmc$ and $C2/c$ ($Cmcm$ and $P\bar{3}1c$), but no evidence for either was found in the S-XRD data. The direct phase transition from $P6_3/mmc$ to $C2/c$ has been observed and carefully studied for 6H-type $Ba_3BSb_2O_9$ (B=Ca, Sr) [16], $Ba_3NdRu_2O_9$ [21], $Ba_3BiRuIrO_9$ [19], and $Ba_3NaIr_2O_9$ [22], with the intermediate $Cmcm$ phase being observed in such phases only for $Ba_3CuRu_2O_9$ [23], $Ba_3NaRu_2O_9$ (below 210 K) [24], and $Ba_3CoRu_2O_9$ (below 2 K) [25]. This symmetry lowering pathway principally involves octahedral rotations about the (110) direction of the hexagonal cell which is equivalent to the (010) direction of the monoclinic cell, as can clearly be seen in Fig. 7, and is driven by the need to alleviate underbonding of Ba cations in the A-sites while maintaining acceptable B–O bond lengths in the BO_6 octahedra. The BVS values show that the room temperature $C2/c$ structure satisfies the bonding requirements of all atoms extremely well, with the sole exception of Bi^{3+}, which appears to be slightly overbonded while still lying within the range commonly observed.

The anisotropic ADPs of $Ba_3LaIr_2O_9$ at 700 K (Fig. 10) indicate that this phase is starting to distort *via* the same symmetry lowering modes as $Ba_3BiIr_2O_9$, rather than the alternate pathway from $P6_3/mmc$ to $P6_3/m$ [26], which involves rotations about the (001) direction of hexagonal cell. However, it appears that the distortions cannot be accommodated coherently in this case, with the structure becoming increasingly strained while essentially remaining in $P6_3/mmc$ as it cools. BVS reported in Table 3 show the need for these distortions in the extreme underbonding of the A-site Ba^{2+} cations and overbonding of the B-site $Ir^{4.5+}$ cations, situations that are almost perfectly corrected for in the $C2/c$ structure of $Ba_3BiIr_2O_9$ (Table 2). The fact that only the latter structure can successfully distort in this way, despite the identical effective ionic radii of La^{3+} and Bi^{3+} in 6-fold coordination (1.03 Å) [27], may be due to the greater polarizability of Bi^{3+} with its stereochemically active $6s^2$ electron lone pair. This explanation is supported by the fact that Bi^{3+} is the least satisfactorily bonded ion (according to BVS) in the room temperature $C2/c$ structure of $Ba_3BiIr_2O_9$. However, this explanation must be considered speculative, as we have been unable to identify any other pair of Bi/La perovskites showing the same contrasting behaviors.

The behavior of $Ba_3LaIr_2O_9$ is similar to (although less extreme than) that observed for $Ba_3BaSb_2O_9$ [28], which also remains in $P6_3/mmc$ as it cools, becoming increasingly strained below an apparent lower stability limit of 923 K, and finally decomposing below 600 K.

5. Conclusions

Two distinct perovskite-type phases exist in the Ba–Bi–Ir–O system: a rock-salt ordered double perovskite Ba_2BiIrO_6; and a 6H-type hexagonal perovskite $Ba_3BiIr_2O_9$. Both phases distort from their ideal high-temperature parent structures on cooling. Ba_2BiIrO_6 undergoes a series of phase transitions $Fm\bar{3}m \rightarrow R\bar{3}c \rightarrow I2/m(C2/m) \rightarrow I\bar{1}(P\bar{1})$, of which the rhombohedral→monoclinic one is first order, resulting in a 2-phase rhombohedral +monoclinic temperature. The fact that this transition and associated 2-phase region lie very close to 300 K, making structural characterization at room temperature extremely difficult, may explain why Ba_2BiIrO_6 has not previously been reported even though it is likely to have been synthesized in the course of published studies of closely related systems. A solid solution $Ba_2Bi_{1+x}Ir_{1-x}O_6$, analogous to $Ba_2Bi_{1+x}Ru_{1-x}O_6$, $0 \le x \le 2/3$ [8], was not observed.

$Ba_3BiIr_2O_9$ undergoes a second-order phase transition $P6_3/mmc \rightarrow C2/c$ at 750 K. The same transition was expected for 6H-type $Ba_3LaIr_2O_9$, previously reported in $C2/c$ at room temperature. However, a re-examination of $Ba_3LaIr_2O_9$ using S-XRD data found that its hexagonal structure is highly strained below ~750 K but fails to distort coherently to the monoclinic phase.

Acknowledgments

This project was supported by the Australian Research Council – Discovery Projects (DP0666465).

References

[1] I. Thumm, U. Treiber, S. Kemmlersack, Journal of Solid State Chemistry 35 (1980) 156.
[2] L. Katz, R. Ward, Inorganic Chemistry 3 (1964) 205.
[3] E.M. Ramos, I. Alvarez, R. Saezpuche, M.L. Veiga, C. Pico, Journal of Alloys and Compounds 225 (1995) 212.
[4] M. Wakeshima, D. Harada, Y. Hinatsu, Journal of Alloys and Compounds 287 (1999) 130.
[5] Y. Doi, Y. Hinatsu, Journal of Solid State Chemistry 177 (2004) 3239.
[6] Y. Doi, Y. Hinatsu, Journal of Physics: Condensed Matter 16 (2004) 2849.
[7] T. Sakamoto, Y. Doi, Y. Hinatsu, Journal of Solid State Chemistry 179 (2006) 2595.
[8] J. Darriet, R. Bontchev, C. Dussarrat, F. Weill, B. Darriet, European Journal of Solid State and Inorganic Chemistry 30 (1993) 273.
[9] M.W. Lufaso, H.C. zur Loye, Inorganic Chemistry 44 (2005) 9154.

[10] B. Hunter, in: International Union of Crystallography Commission on Powder Diffraction Newsletter, vol. 20, 1998.
[11] A.C. Larson, R.B. Von Dreele, Los Alamos National Laboratory Report LAUR 86-748, 1994.
[12] B.H. Toby, Journal of Applied Crystallography 34 (2001) 210.
[13] B.J. Kennedy, C.J. Howard, K.S. Knight, Z.M. Zhang, Q.D. Zhou, Acta Crystallographica Section B: Structural Science 62 (2006) 537.
[14] Q.D. Zhou, B.J. Kennedy, M. Avdeev, L. Giachini, J.A. Kimpton, Journal of Solid State Chemistry 182 (2009) 3195.
[15] C.J. Howard, B.J. Kennedy, P.M. Woodward, Acta Crystallographica Section B: Structural Science 59 (2003) 463.
[16] C.D. Ling, B. Rowda, M. Avdeev, R. Pullar, Journal of Solid State Chemistry 182 (2009) 479.
[17] N.E. Brese, M. O'Keeffe, Acta Crystallographica Section B 47 (1991) 192.
[18] J. Darriet, R. Bontchev, C. Dussarrat, F. Weill, B. Darriet, European Journal of Solid State and Inorganic Chemistry 30 (1993) 287.
[19] M.W. Lufaso, H.C. zur Loye, Solid State Sciences 8 (2006) 1051.
[20] M.I. Aroyo, J.M. Perez-Mato, C. Capillas, E. Kroumova, S. Ivantchev, G. Madariaga, A. Kirov, H. Wondratschek, Zeitschrift Fur Kristallographie 221 (2006) 15.
[21] Y. Doi, Y. Hinatsu, Y. Shimojo, Y. Ishii, Journal of Solid State Chemistry 161 (2001) 113.
[22] H.C. zur Loye, S.J. Kim, R. Macquart, M.D. Smith, Y. Lee, T. Vogt, Solid State Sciences 11 (2009) 608.
[23] J.T. Rijssenbeek, Q. Huang, R.W. Erwin, H.W. Zandbergen, R.J. Cava, Journal of Solid State Chemistry 146 (1999) 65.
[24] K.E. Stitzer, M.D. Smith, W.R. Gemmill, H.C. zur Loye, Journal of the American Chemical Society 124 (2002) 13877.
[25] P. Lightfoot, P.D. Battle, Journal of Solid State Chemistry 89 (1990) 174.
[26] H.W. Zandbergen, D.J.W. Ijdo, Acta Crystallographica Section C: Crystal Structure Communications 39 (1983) 829.
[27] R.D. Shannon, Acta Crystallographica Section A 32 (1976) 751.
[28] C.D. Ling, M. Avdeev, K. Aivazian, Acta Crystallographica Section B: Structural Science 63 (2007) 584.